Supporting information

Visible-light driven catalase-like activity of blackberry-shaped $\{Mo_{72}Fe_{30}\}$ nanovesicles: combined kinetic and mechanistic studies

Rezvan Mokhtari, Abdolreza Rezaeifard,* Maasoumeh Jafarpour,* and Alireza Farrokhi

Experimental

General remarks:

All chemicals were purchased from Merck and Across Chemical Companies. Household full-spectrum 40 W compact fluorescent light (CFL) bulb used as visible light irradiation source in combination with some filters. Powder X-ray diffraction (XRD) was performed on a Bruker D8-advance X-ray diffractometer and also STOE STAD IP with Cu Ka (λ= 1.5406 Å) radiation. The FT-IR spectra were recorded on a Shimadzu 800 FT-IR and also a JASCO FT-IR 4600 system using a KBr pellet. Raman spectra were recorded on a Takram P50C0R10 spectrometer and also Nicolet Almega Y dispersive. The BET surface area was detected by the nitrogen adsorption-desorption measurements, which were measured at 77 K on a Belsorp-mini II (Bel Japan). Diffuse reflectance spectra (DRS) were obtained with an Avant's spectrophotometer *(*Avaspec-2048-TEC*)*. TEM images were obtained by Department of Electron Microscopy Zeiss EM-10 West Germany. SEM performed by Scanning Electron Microscope TESCAN Vega Model and also by FEG-HR-SEM SU8220 from HITACHI with EDX detector (Bruker) for elemental analysis. Magnetic susceptibility measurements were made by using a Lake Shore 7400 magnetometer at a field of 1 Tesla in 298 K. UV-Vis spectrum were recorded on a SPECORD®210 PLUS spectrophotometer. The TGA measurements were obtained by a TGA-50 (Shimadzu) at the heating rate of 10 °C/min under 20 mL/min flowing air. The DLS measurements were obtained by Malvern Instruments Ltd, DTS Ver. 5.02, Serial Number: MAL1033451 with Glass cuvette with square aperture at 25 ºC and measurement position of 1.25 mm. The EPR spectra were recorded at 9.75 GHz (X-band) on a Bruker ELEXSYS E580 using a Bruker 4119HS-W1 resonator. All EPR spectra where recorded using a modulation frequency of 100 kHz, modulation amplitude of 10 G, and a microwave attenuation of 20 dB (1.5 mW). HQ40d portable dissolved oxygen meter with digital readout

(HACH Company) was used to measure the amount of produced oxygen during the reaction. The intensity of irradiations in photochemical experiments was measured by a lux meter (TES-1339R, Data Logger Light Meter Pro).

Synthesis of Amorphous {$Mo_{72}Fe_{30}$}[1]

2.09 g $FeCl_3.6H_2O$ (7.7 mmol) was added under vigorous stirring to a solution of 3 g $Na_2MoO_4.2H_2O$ (12.3 mmol) in 25 mL water acidified with 15 mL of 100 % acetic acid (final pH ca. 2) led to immediate precipitation. The yellow precipitate was filtered off after 30 min, thoroughly washed with water and dried in air. The yellow solid characterized by FT-IR (Fig. S1), Raman (Fig. S2), UV-Vis (Fig. S3), XRD (Fig. S4), TGA (Fig. S5), EDS (Fig. S6), VSM (Fig. S7), SEM, TEM (Fig. 4) and BET (Fig. S21).

Synthesis of Crystalline {$Mo_{72}Fe_{30}$}[2]

To a stirred orange-red solution of 1.1 g $FeCl_3.6H_2O$ (4.1 mmol) and 1.1 g $CH_3COONa.3H_2O$ (8.1 mmol) in 75 mL H_2O, 1.4 g the ammonium salt of {Mo_{132}} (0.05 mmol) was added. The resulting mixture was vigorously stirred in an open 100-mL Erlenmeyer flask (wide-necked) for 24 h. After acidification with HCl (1M, 1 mL) and addition of NaCl (2.0 g), the stirred reaction mixture was heated to 90 - 95 °C and then filtered whilst still hot. The golden yellow filtrate was cooled to 20 °C, and yellow crystals formed over a period of 2 - 3 days. The crystals were collected by filtration through a glass frit, washed twice with a little iced water (to remove the adhering NaCl), and dried in air. The yellow crystals characterized by FT-IR (Fig. S8), Raman (Fig. S9), XRD (Fig. S10), EDS (Fig. S11), TGA (Fig. S12), SEM (Fig. S13) and TEM (Fig. S14).

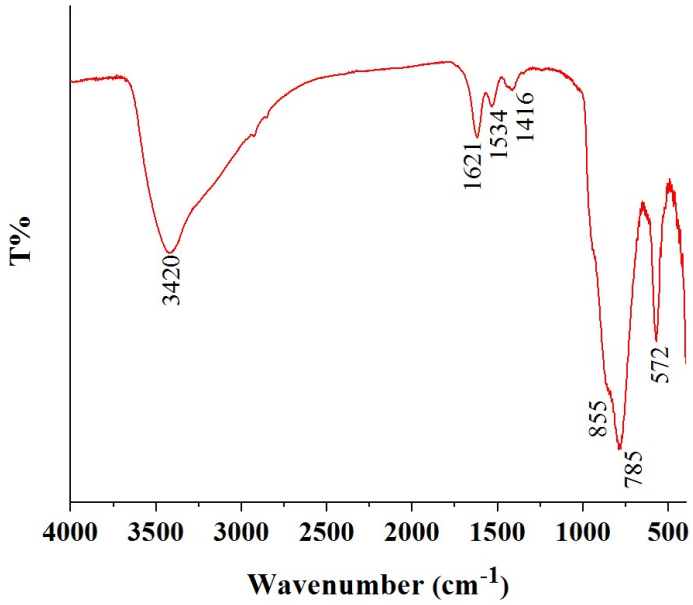

Fig. S1. FT-IR spectra of amorphous $\{Mo_{72}Fe_{30}\}$

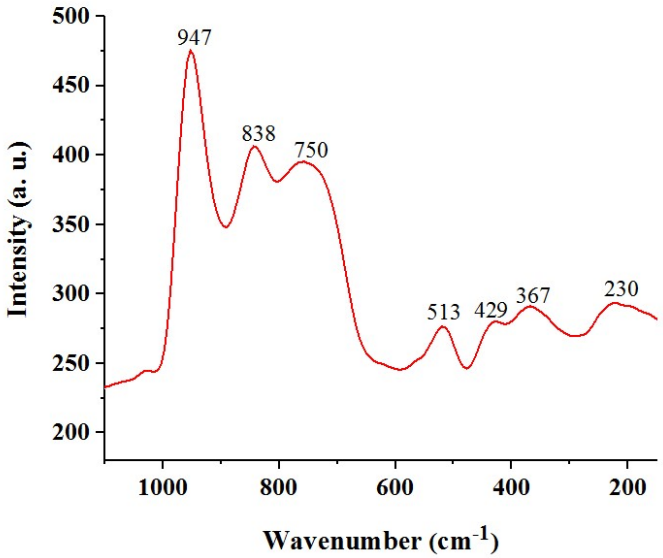

Fig. S2. The Raman spectrum of amorphous $\{Mo_{72}Fe_{30}\}$

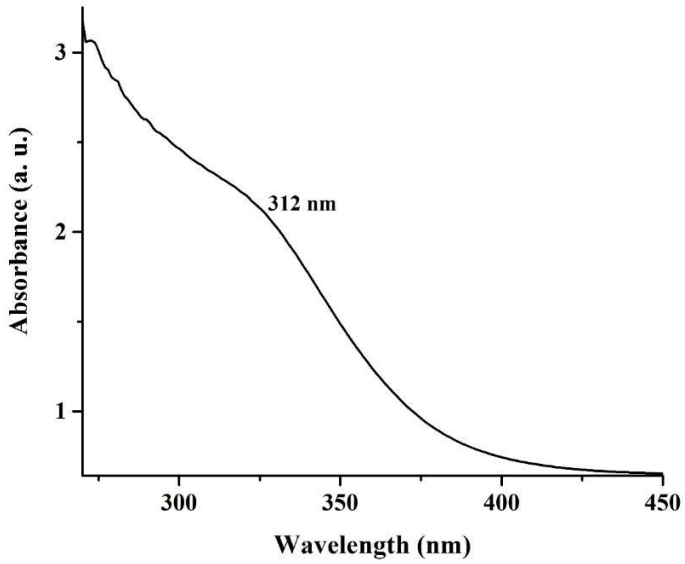

Fig. S3. The UV-Vis spectra of amorphous $\{Mo_{72}Fe_{30}\}$ in DMSO

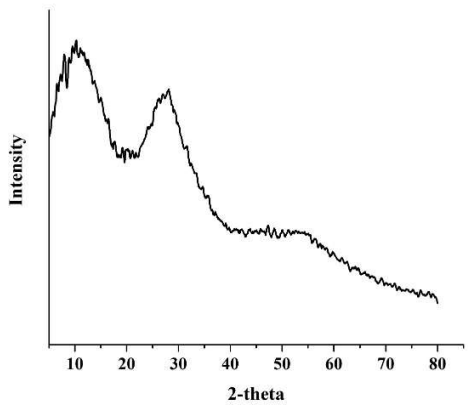

Fig. S4. X-ray diffraction pattern of amorphous $\{Mo_{72}Fe_{30}\}$

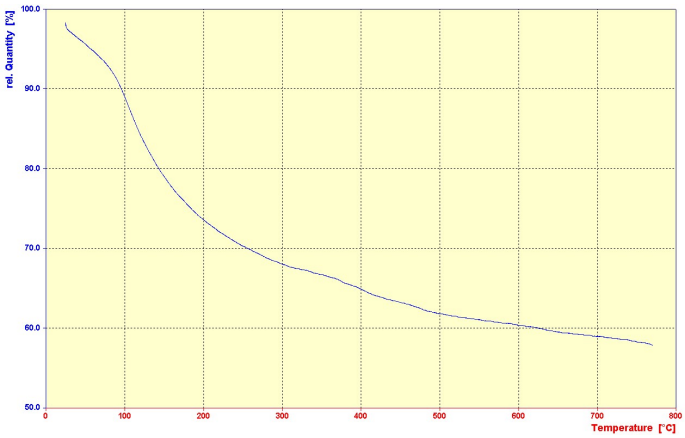

Fig. S5. The TGA of amorphous $\{Mo_{72}Fe_{30}\}$ nanocluster; The first stage of water removal is observed up to ~100°C and results in a 7% weight loss. Then there is second stage of water and carbon dioxide (360°C) removal. The weight loss was 27%.

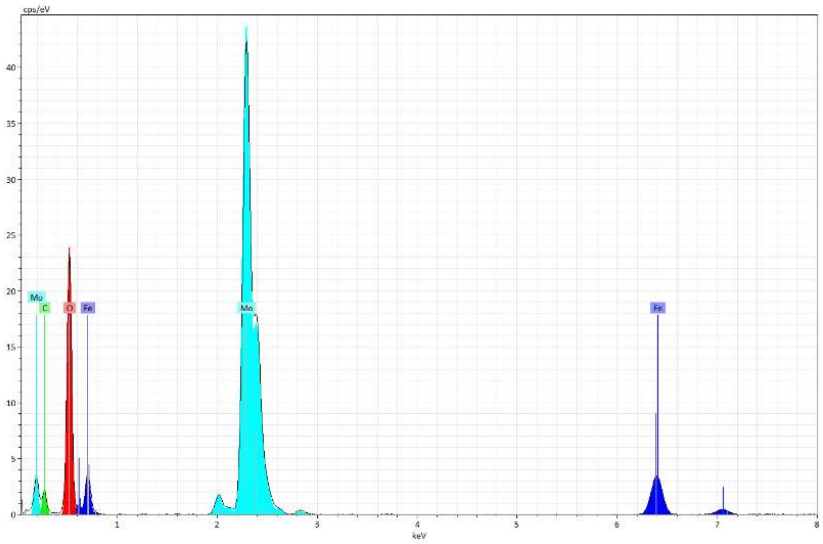

Element	W%	A%
C	5.15	11.72
O	41.45	70.85
Fe	10.72	5.25
Mo	42.68	12.18

Fig. S6. EDS elemental analysis of amorphous $\{Mo_{72}Fe_{30}\}$

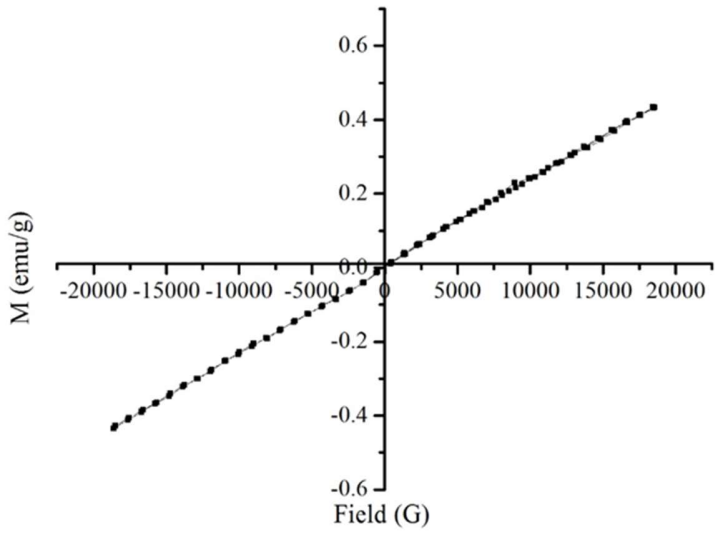

Fig. S7. Magnetization curve of amorphous $\{Mo_{72}Fe_{30}\}$

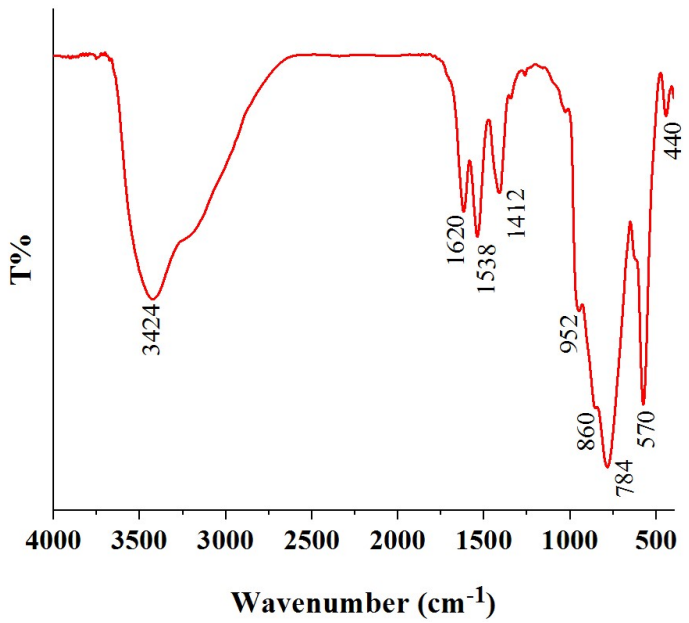

Fig. S8. FT-IR spectra of crystalline $\{Mo_{72}Fe_{30}\}$

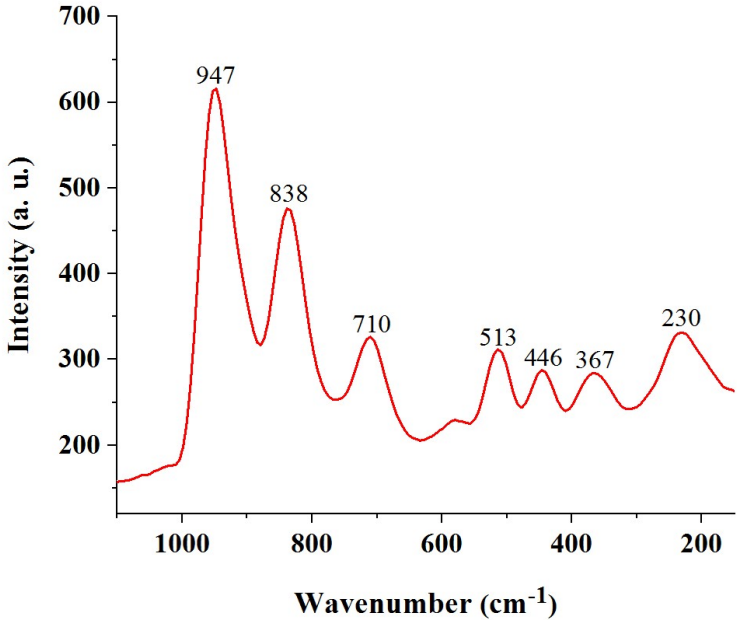

Fig. S9. Raman spectra of crystalline $\{Mo_{72}Fe_{30}\}$

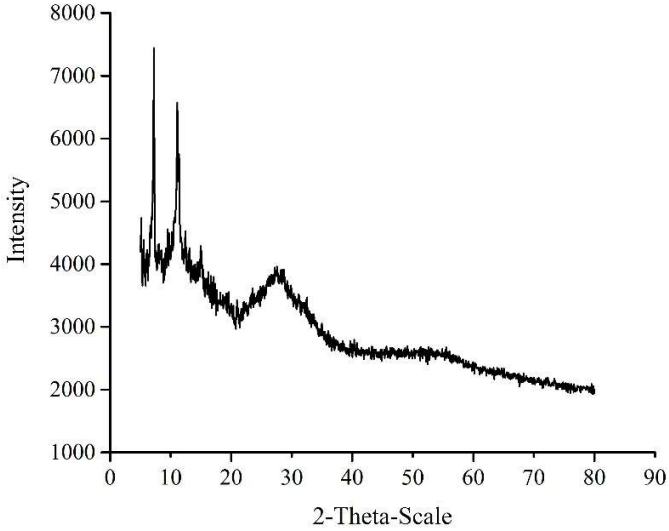

Fig. S10. X-ray diffraction pattern of crystalline $\{Mo_{72}Fe_{30}\}$.

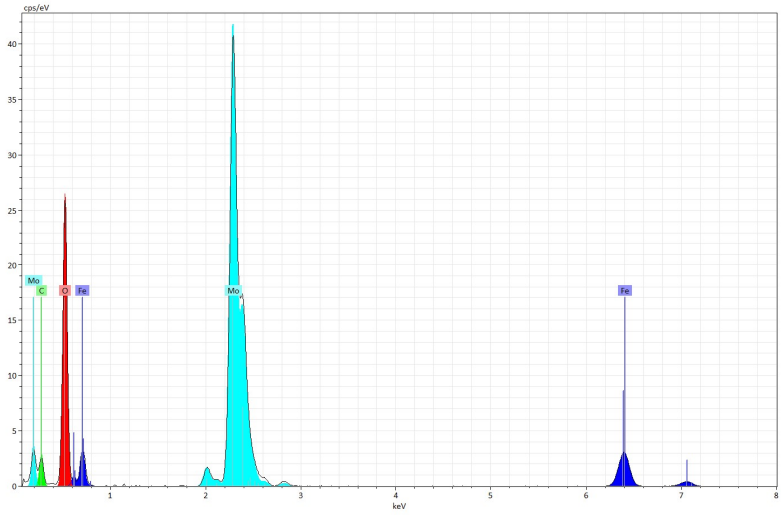

Element	W%	A%
C	5.72	12.85
O	41.65	70.32
Fe	9.91	4.80
Mo	42.72	12.03

Fig. S11. EDX analysis of crystalline $\{Mo_{72}Fe_{30}\}$

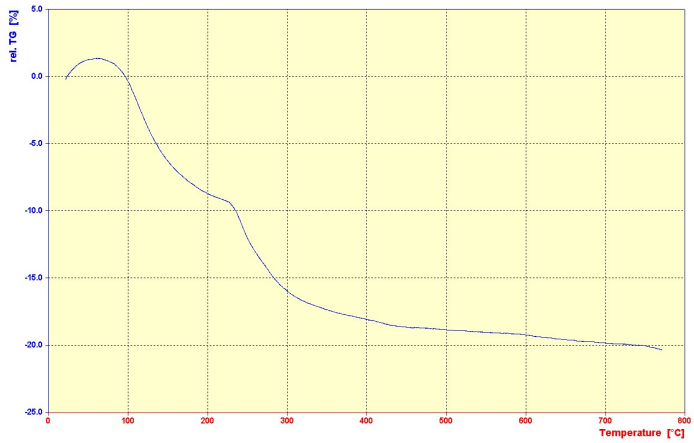

Fig. S12. The TGA of crystalline $\{Mo_{72}Fe_{30}\}$

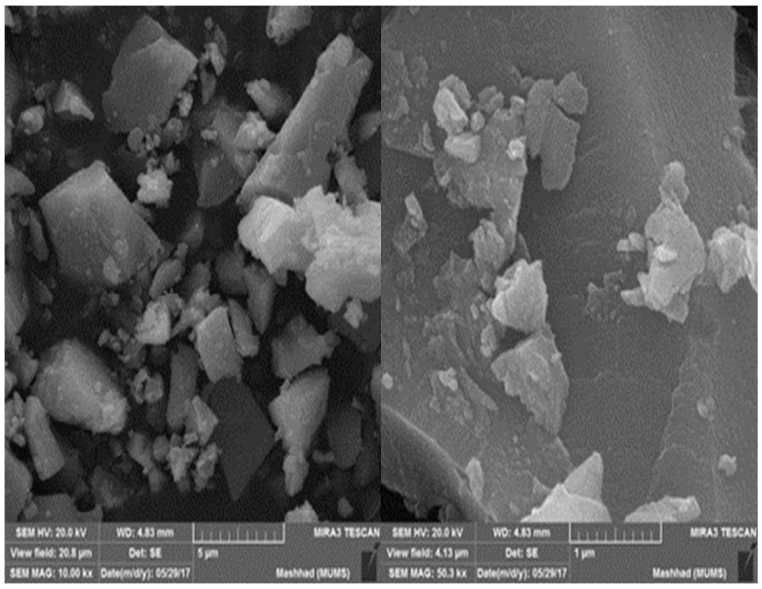

Fig. S13. SEM image of crystalline $\{Mo_{72}Fe_{30}\}$

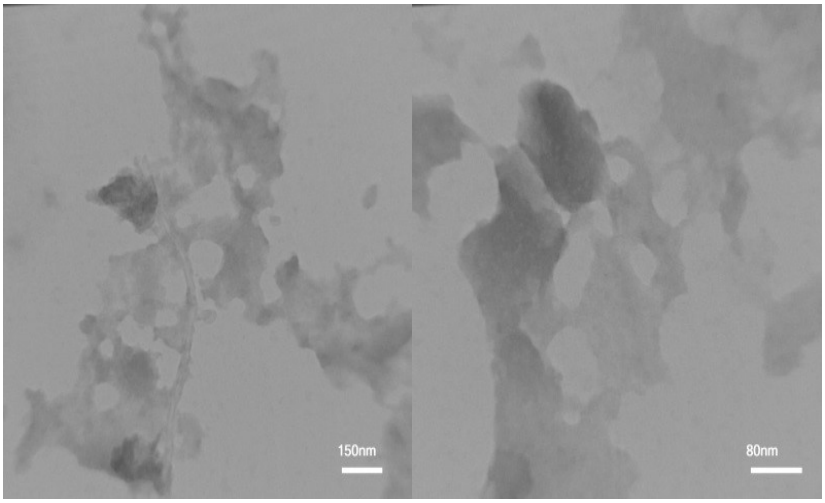

Fig. S14. TEM image of crystalline $\{Mo_{72}Fe_{30}\}$

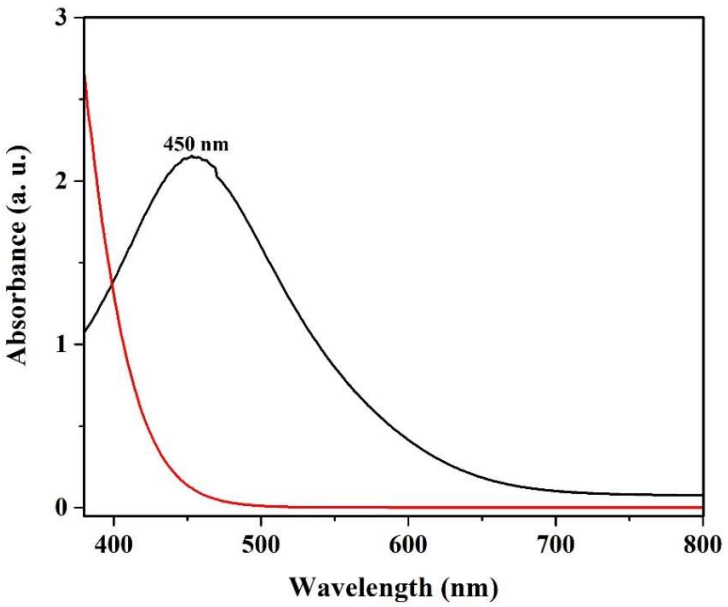

Fig. S15. UV-Vis spectra of $\{Mo_{132}\}$ before (black line) and after reaction (red line) with 20 mM H_2O_2.

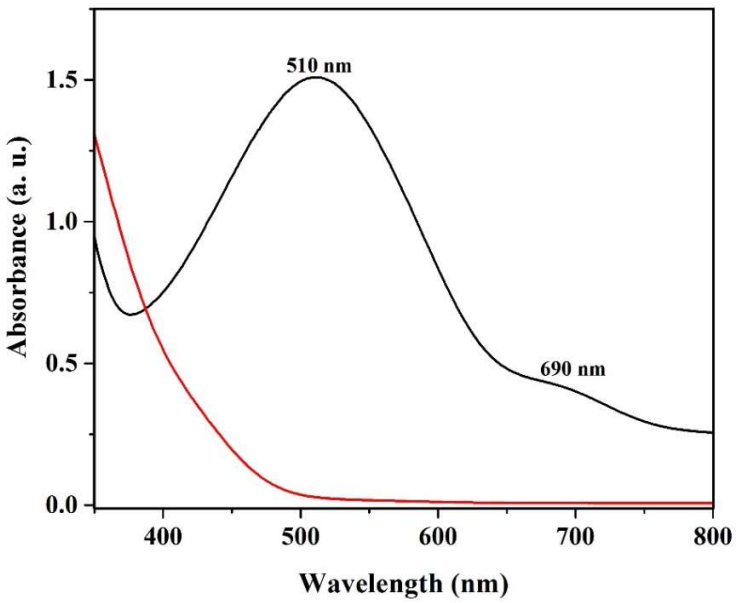

Fig. S16. UV-Vis spectra of $\{Mo_{72}V_{30}\}$ before (black line) and after reaction (red line) with 20 mM H_2O_2.

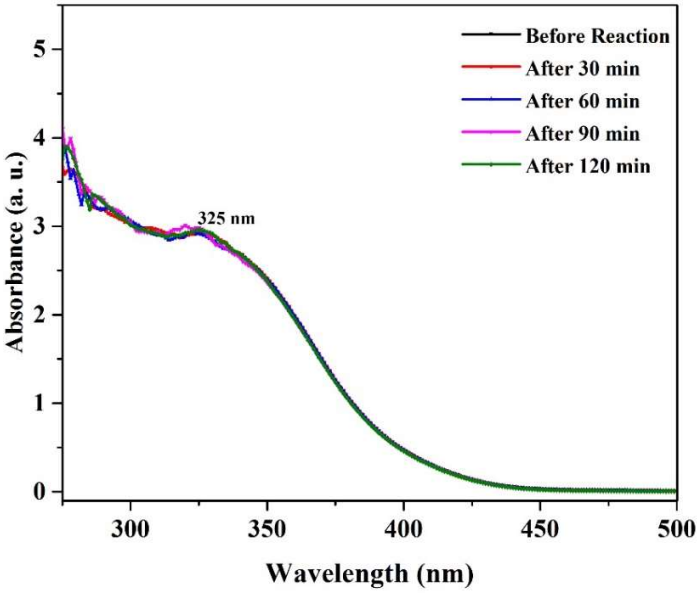

Fig. S17. UV-Vis spectra of crystalline $\{Mo_{72}Fe_{30}\}$ before and after reaction with H_2O_2 at different time intervals. Reaction conditions: 10 ml of acetate buffer (0.1 M, pH = 3); $[H_2O_2]$ = 20 mM; $\{Mo_{72}Fe_{30}\}$ = 0.08 μmol (8μM); T= 298 K.

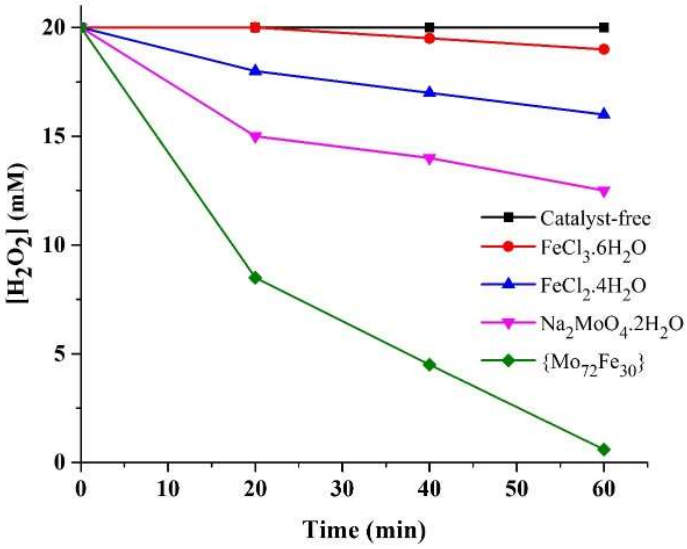

Fig. S18. Time course decomposition of H_2O_2 under visible-light irradiation (CFL bulb). Reaction conditions: 10 mL of buffered solution (acetate 0.1 M, pH = 3) of 20 mM H_2O_2 at 298 K containing 6 mg (0.32 μmol) amorphous $\{Mo_{72}Fe_{30}\}$, 0.010 mmol $FeCl_3.6H_2O$ and $FeCl_2.4H_2O$ and 0.023 mmol $Na_2MoO_4.H_2O$.

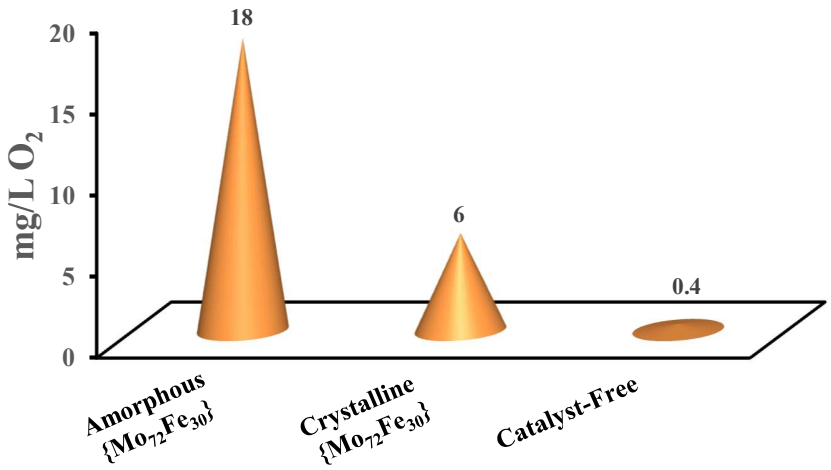

Fig. S19. O_2 production by H_2O_2 decomposition in the absence and presence of amorphous and crystalline $\{Mo_{72}Fe_{30}\}$ detected by dissolved oxygen sensor. Reaction conditions: 10 ml of acetate buffered solution (0.1 M, pH=3) of 10 mM H_2O_2 containing 1 μmol $\{Mo_{72}Fe_{30}\}$ at 298 K.

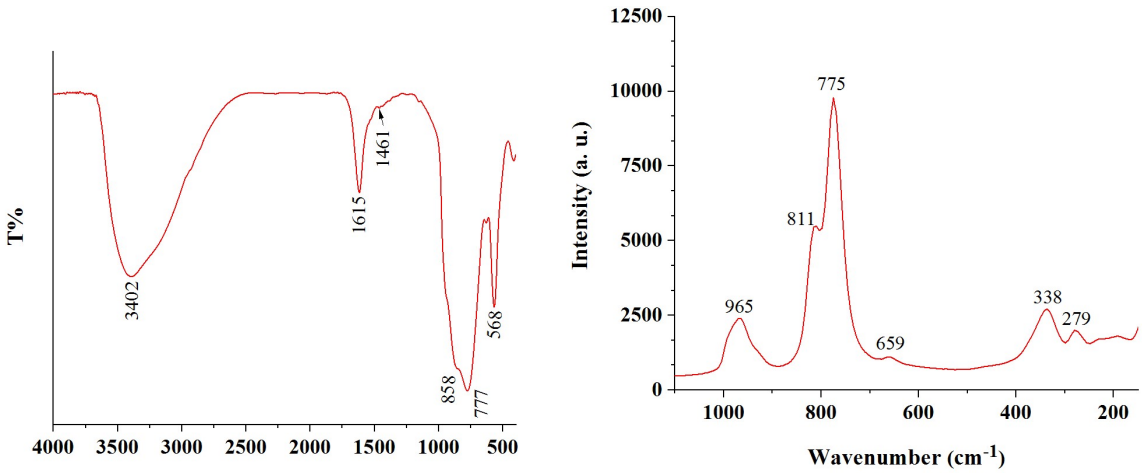

Fig. S20. FT-IR (left) and Raman spectra (right) of amorphous $\{Mo_{72}Fe_{30}\}$ after treatment with H_2O_2 in neutral conditions (pH≥6.6) and in the presence of high concentration of H_2O_2 (>70 mM)

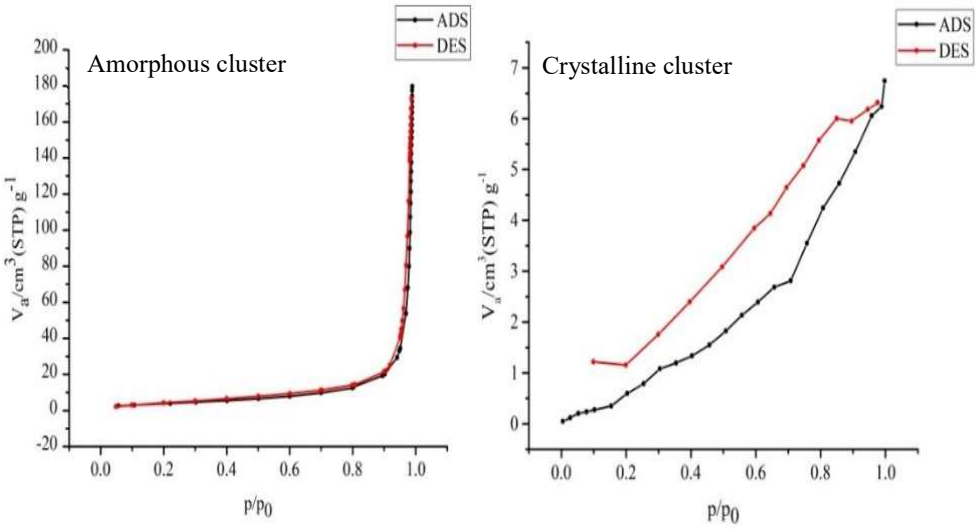

Fig. S21. N_2 adsorption–desorption isotherms of amorphous and crystalline $\{Mo_{72}Fe_{30}\}$

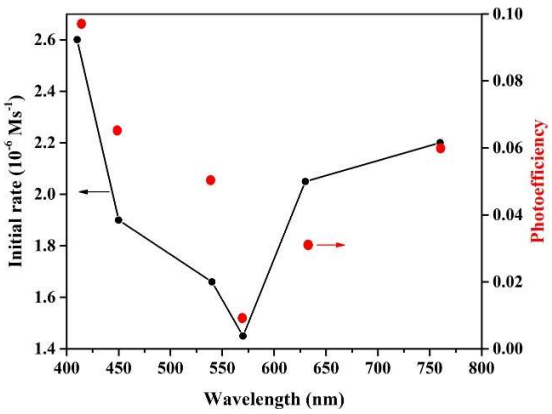

Fig S22. Initial rate (black circle) and photoefficiency (red circle) of the H_2O_2 (20 mM) decomposition in a buffered solution (acetate, 0.1 M, pH=3) containing 6 mg (0.32 μmol) amorphous $\{Mo_{72}Fe_{30}\}$ under visible light irradiation (CFL lamp) at different wavelengths (415, 450, 530, 570, 630 and 760 nm) at 298 K.

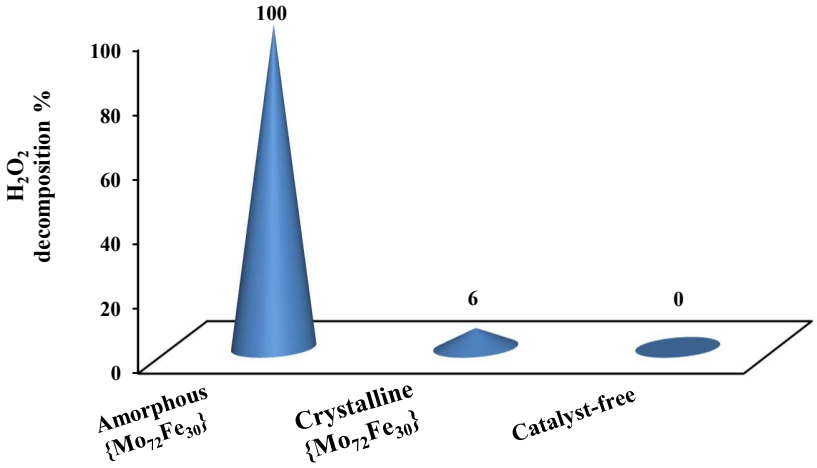

Fig. S23. Solar photocatalytic activity of amorphous and crystalline {$Mo_{72}Fe_{30}$} in H_2O_2 decomposition after 30 min. Reaction conditions: 10 mL of buffered solution (acetate 0.1 M, pH=3) of 20 mM H_2O_2 containing 6 mg (0.32 μmol) of amorphous {$Mo_{72}Fe_{30}$} at 298 K under sun light.

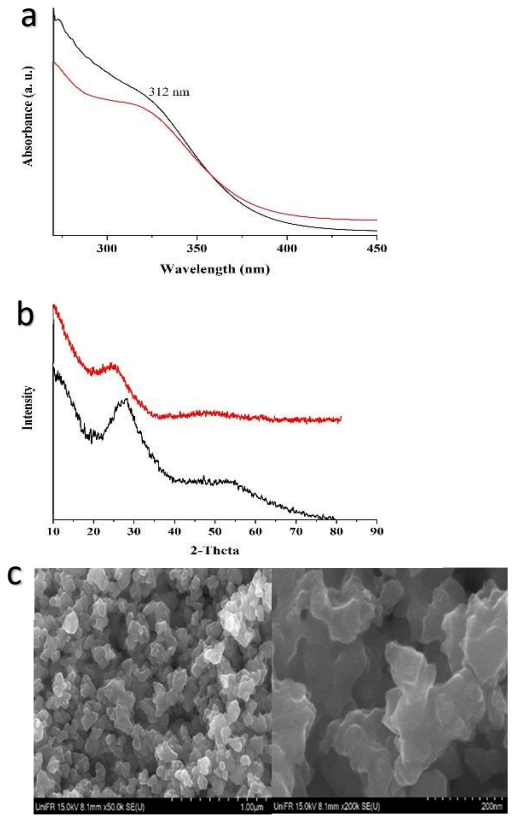

Fig. S24. (a) UV-Vis spectra in DMSO (b) PXRD pattern and (c) HR-SEM images of used amorphous {$Mo_{72}Fe_{30}$} after recovery from the aqueous solution of 20 mM H_2O_2 at 298K.

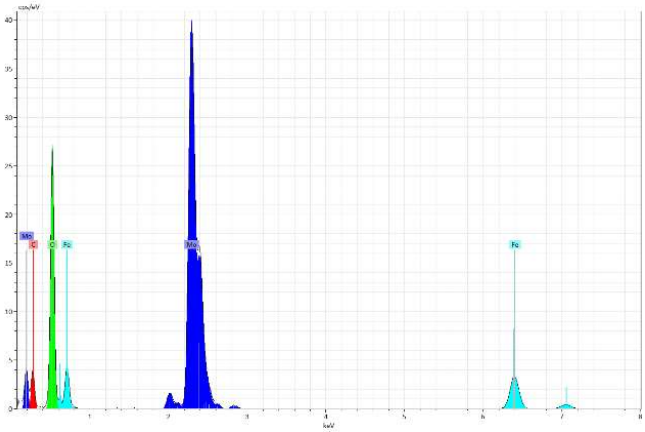

Element	W%	A%
C	5.18	11.80
O	41.28	70.61
Fe	11.33	5.55
Mo	42.21	12.04

Fig. S25. EDS elemental composition of used amorphous $\{Mo_{72}Fe_{30}\}$ cluster after treatment with 20 mM buffered solution (acetate 0.1 M, pH = 3) of H_2O_2 (pH=3)

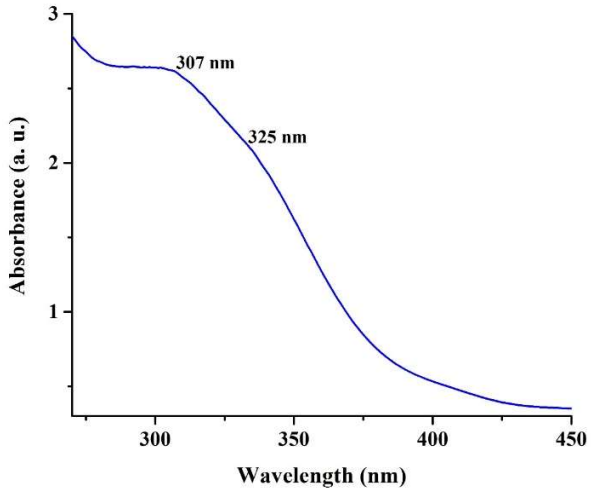

Fig. S26. The UV/Vis spectra of aqueous suspension of amorphous $\{Mo_{72}Fe_{30}\}$ containing H_2O_2 (20 mM) at buffered solution (acetate 0.1 M, pH = 3).

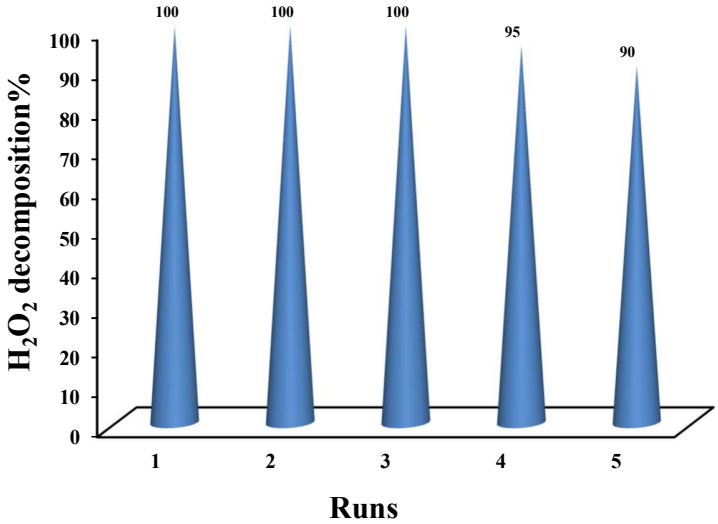

Fig. S27. Recycling of the catalytic system based on H_2O_2 decomposition using permanganate titration. Reaction conditions: 10 mL of buffered solution (acetate 0.1 M, pH = 3) of 20 mM H_2O_2 containing 6 mg (0.32 μmol) of amorphous $\{Mo_{72}Fe_{30}\}$ at 298 K under day light.

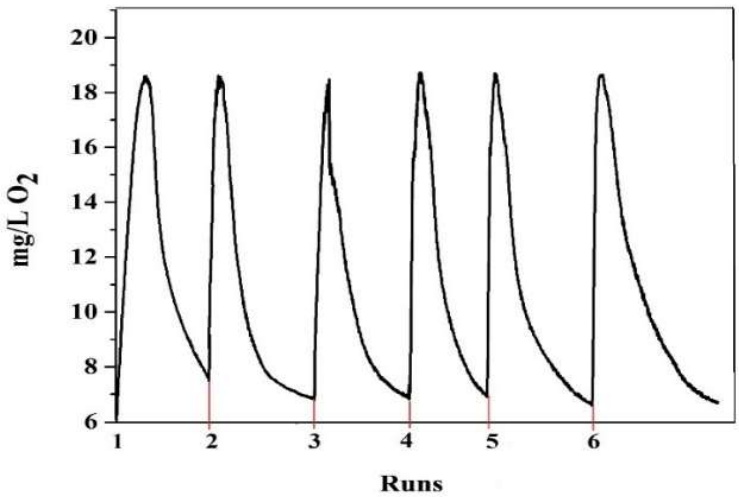

Fig. 28. Recyclability of the catalytic system based on O_2 production using dissolved oxygen measurement. Reaction condition: Injection of 10 μL of 30% H_2O_2 to10 mL of buffered solution (acetate 0.1 M, pH = 3) containing 6 mg (0.32 μmol) of amorphous $\{Mo_{72}Fe_{30}\}$ at 298 K under CFL light for each run.

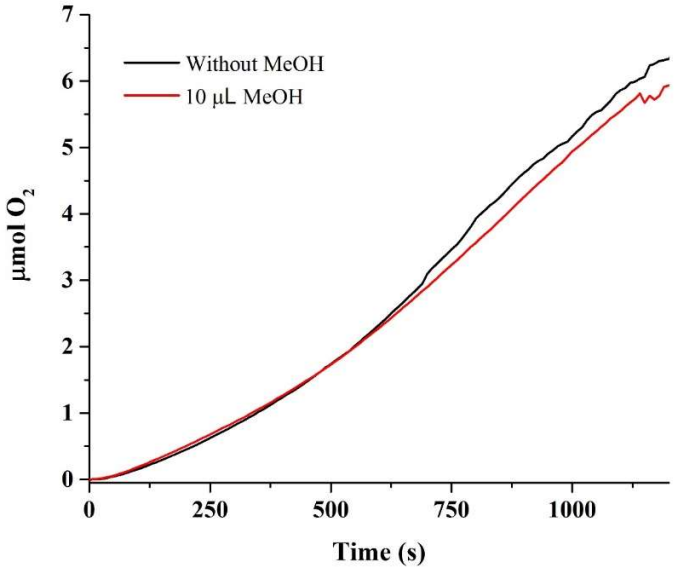

Fig. S29. O_2 production by H_2O_2 decomposition in the absence and presence of MeOH as hydroxyl radical scavenger. Reaction conditions: 20 mM H_2O_2, 0.32 μmol $\{Mo_{72}Fe_{30}\}$, 10 μL (25 mM) MeOH, T= 298 K at 10 mL buffered solution (acetate 0.1 M, pH = 3).

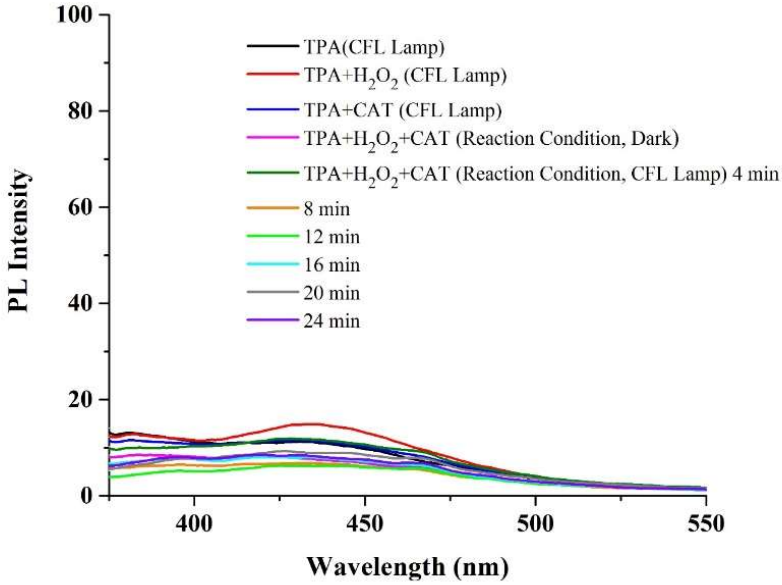

Fig. S30. The photoluminescence spectra of 2-hydroxy-terephthalic acid formed by the reaction of terephthalic acid (TPA) with $^{\bullet}OH$ radicals generated from different samples and at different time irradiation. Reaction conditions: 0.32 μmol (6 mg) of $\{Mo_{72}Fe_{30}\}$ (CAT), 10 mL of 0.02 M H_2O_2 buffered solution (acetate 0.1 M, pH = 3) at 298 K, 5×10^{-4} M terephthalic acid solution in NaOH (2×10^{-3} M).

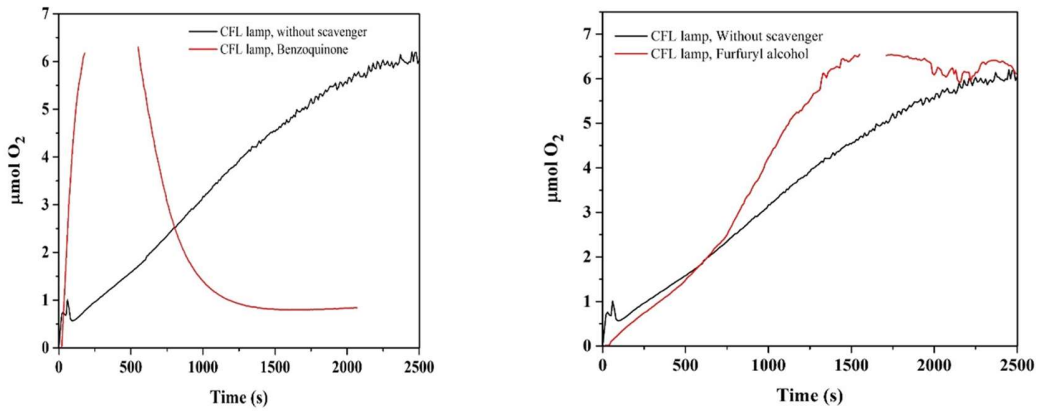

Fig. S31. O_2 production by H_2O_2 decomposition in the absence and presence of benzoquinone as peroxide radical scavenger (left) and furfuryl alcohol as singlet oxygn scavenger (right) in equimolar concentration with respect to H_2O_2. Reaction conditions: 20 mM H_2O_2, 0.32 µmol $\{Mo_{72}Fe_{30}\}$, T= 298 K at 10 mL buffered solution (acetate 0.1 M, pH = 3).

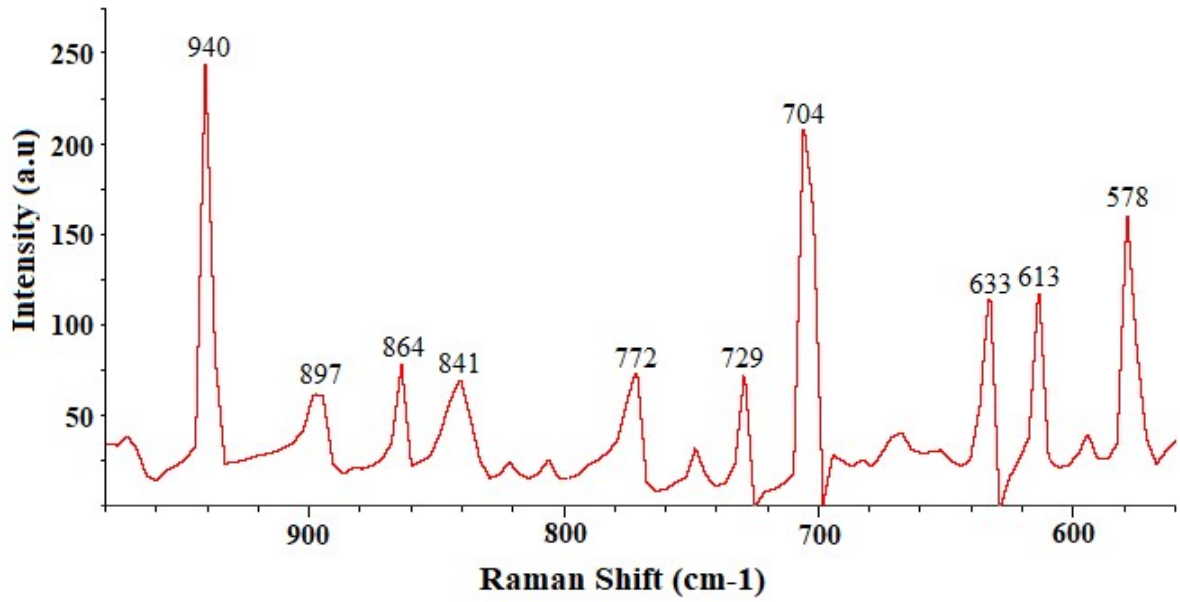

Fig. S32. Raman spectra of amorphous $\{Mo_{72}Fe_{30}\}$ (1 µmol) in the buffered solution (acetate 0.1 M, pH = 3) of 20 mM H_2O_2 at T= 298 K after 15 min irradiation under visible light.

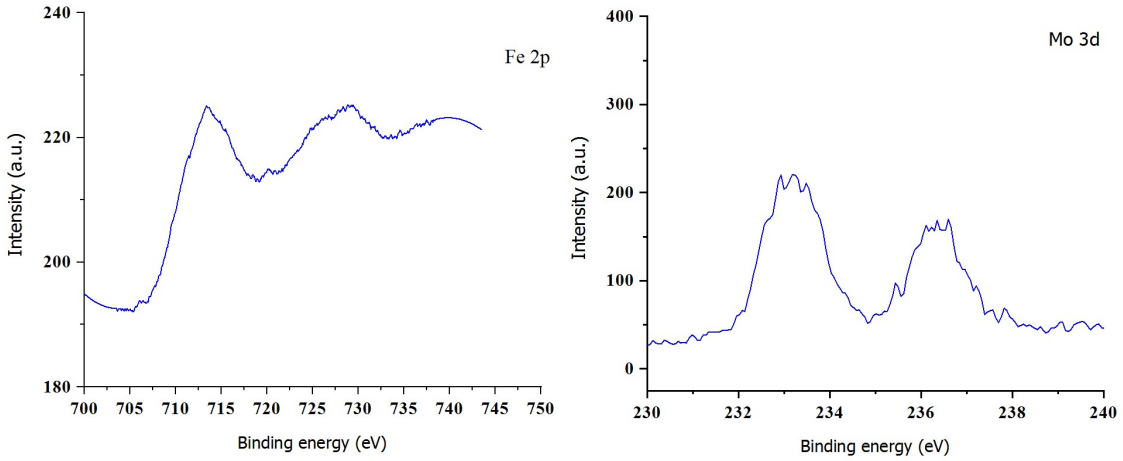

Fig. S33. Fe 2p and Mo 3d XPS of used amorphous $\{Mo_{72}Fe_{30}\}$

Table S1. Comparison of catalytic activity of amorphous $\{Mo_{72}Fe_{30}\}$ with other catalysts used in dismutation of H_2O_2 (mainly through catalase-like mechanism).

Entry	Catalyst	$[H_2O_2]$ mM	System type	pH	Initial rate (μmol O_2 s^{-1})	TOF (s^{-1})	TON[a] (Time/ min)	Ref
1	$Ru_4(SiW_{10})_2$	33	Homogeneous	7	0.20	1.27	3050 (100)	3
2	$Cu_4(PW_9)_2$	33	Homogeneous	7	1.53×10^{-2}	-	79 (30)	3
3	$Co_4(PW_9)_2$	33	Homogeneous	7	1.2×10^{-3}	-	14 (30)	3
4	$Ni_4(PW_9)_2$	33	Homogeneous	7	0.8×10^{-3}	-	6 (30)	3
5	$Mn_4(PW_9)_2$	33	Homogeneous	7	1.5×10^{-3}	-	9 (30)	3
6	$Fe_4(PW_9)_2$	33	Homogeneous	7	1.1×10^{-3}	-	11 (30)	3
7	$Ru_4(SiW_{10})_2$@ MWCNT[b]	33	Heterogeneous	7	3.64×10^{-2}	-	1050(100)	3
8	$Ru_4(SiW_{10})_2$@ PANI[c]	33	Heterogeneous	7	4.24×10^{-2}	-	1750 (100)	3
9	$Ru_4(SiW_{10})_2$@ PDDA[d]	33	Heterogeneous	7	7.7×10^{-2}	-	2200 (100)	3
10	$[Mn^{IV}V_{13}O_{38}]^{7-}$	1	Homogeneous	3.8	0.26	0.018	200 (180)	4
11	Mn salen, EUK-8	1	Homogeneous	7.8	0.14	0.0068	1.07	5
12	Mn porphyrins 14 examples	1	Homogeneous	7.8	0.126-0.913	0.0063-0.045	3.94-12.54	5
13	$\{Mo_{72}Fe_{30}\}$	10-70	Heterogeneous /Homogeneous	3	0.01[e]	0.03[e]	1450 (60)[f] 3800 (Total)[f]	This work

[a]Moles of decomposed H_2O_2 per moles of catalyst; [b]Multi walled carbon nanotube, [c]Polyaniline, [d]Poly(diallyldimethylammoniumchloride); [e] 70mM H_2O_2, 0.32 μmol $\{Mo_{72}Fe_{30}\}$; [f]20mM H_2O_2, 0.053 μmol $\{Mo_{72}Fe_{30}\}$.

References

1 K. Kuepper, M. Neumann, A. J. M. Al-Karawi, A. Ghosh, S. Walleck, T. Glaser and P. Gouzerh, *J. Clust. Sci.* 2014 ***25*** 301–311.

2 A. Müller, S. Sarkar, S. Q. N. Shah, H. Bögge, M. Schmidtmann, S. Sarkar, P. Kögerler, B. Hauptfleisch, A. X. Trautwein and V. Schünemann, *Angew. Chemie Int. Ed.* 1999, **38** 3238–3241

3 A. Sartorel, M. Truccolo, S. Berardi, M. Gardan, M. Carraro, F. M. Toma, G. Scorrano, M. Prato and M. Bonchio, *Chem. Commun.* 2011, **47** 1716–1718.

4 S. Chakrabarty and R. Banerjee *Catal. Sci. Technol.* 2012, **2** 2224–2226.

5 A.Tovmasyan et al. *Free Radic Biol.Med.* 2015 **86** 308–321.